



# Evaluating different metrics from the thermal-based two-source energy balance model for monitoring grapevine water stress

Héctor Nieto<sup>1,2</sup> · María Mar Alsina<sup>3</sup> · William P. Kustas<sup>4</sup> · Omar García-Tejera<sup>5</sup> · Fan Chen<sup>4</sup> · Nicolas Bambach<sup>6</sup> · Feng Gao<sup>4</sup> · Joseph G. Alfieri<sup>4</sup> · Lawrence E. Hipps<sup>7</sup> · John H. Prueger<sup>8</sup> · Lynn G. McKee<sup>4</sup> · Einar Zahn<sup>9</sup> · Elie Bou-Zeid<sup>9</sup> · Andrew J. McElrone<sup>10</sup> · Sebastian J. Castro<sup>10,11</sup> · Nick Dokoozlian<sup>3</sup>

Received: 11 December 2021 / Accepted: 24 March 2022 / Published online: 16 May 2022  
© The Author(s) 2022

## Abstract

Precision irrigation management requires operational monitoring of crop water status. However, there is still some controversy on how to account for crop water stress. To address this question, several physiological, several physiological metrics have been proposed, such as the leaf/stem water potentials, stomatal conductance, or sap flow. On the other hand, thermal remote sensing has been shown to be a promising tool for efficiently evaluating crop stress at adequate spatial and temporal scales, via the Crop Water Stress Index (CWSI), one of the most common indices used for assessing plant stress. CWSI relates the actual crop evapotranspiration ET (related to the canopy radiometric temperature) to the potential ET (or minimum crop temperature). However, remotely sensed surface temperature from satellite sensors includes a mixture of plant canopy and soil/substrate temperatures, while what is required for accurate crop stress detection is more related to canopy metrics, such as transpiration, as the latter one avoids the influence of soil/substrate in determining crop water status or stress. The Two-Source Energy Balance (TSEB) model is one of the most widely used and robust evapotranspiration model for remote sensing. It has the capability of partitioning ET into the crop transpiration and soil evaporation components, which is required for accurate crop water stress estimates. This study aims at evaluating different TSEB metrics related to its retrievals of actual ET, transpiration and stomatal conductance, to track crop water stress in a vineyard in California, part of the GRAPEX experiment. Four eddy covariance towers were deployed in a Variable Rate Irrigation system in a Merlot vineyard that was subject to different stress periods. In addition, root-zone soil moisture, stomatal conductance and leaf/stem water potential were collected as proxy for in situ crop water stress. Results showed that the most robust variable for tracking water stress was the TSEB derived leaf stomatal conductance, with the strongest correlation with both the measured root-zone soil moisture and stomatal conductance gas exchange measurements. In addition, these metrics showed a better ability in tracking stress when the observations are taken early after noon.

## Introduction

Monitoring crop water stress is crucial for irrigation management. Particularly for tree and vine crops, inducing a regulated water stress at certain phenological stages has been shown to positively affect fruit quality (Bravdo et al. 1985; Lopez et al. 2012). Regulated deficit irrigation (RDI) is a strategy that is typically used in viticulture to submit vines to a slight to moderate stress. Precise irrigation practices in viticulture, therefore, should account for a near-real-time monitoring of plant stress that could help in triggering/

suppressing irrigation according to the RDI plan. Traditionally, crop stress has been defined from measurements of water potential  $\Psi$ , either leaf, stem or pre-dawn (Flexas et al. 2004), measured in situ with a pressure chamber (Scholander et al. 1965). However, several authors pointed out the pitfalls or issues regarding the use of water potential measurements at leaf level for irrigation scheduling, as those  $\Psi$  thresholds are point based and are likely to vary depending on root distribution, vine vigour, leaf area index, soil texture variations and/or physiological and morphological responses to water stress (van Leeuwen et al. 2009; Romero et al. 2010; García-Tejera et al. 2021).

As one alternative, previous studies have suggested other proxies, such as the use of stomatal conductance ( $g_s$ ) or sap flow measurements (Eastham and Gray 1998; Ginestar et al.

✉ Héctor Nieto  
hector.nieto@ica.csic.es

Extended author information available on the last page of the article

1998; Patakas et al. 2005), considering these as a more precise and sensitive indicator of water stress than  $\Psi$  (Flexas et al. 2004; Cifre et al. 2005; Romero et al. 2010; Zúñiga et al. 2018). However, measuring these metrics in situ is more challenging due to the need of use of more expensive equipment, a higher level of expertise, and yet still prone to errors (Jarvis 1976).

Remote sensing can be an operational and low-cost alternative for providing spatially distributed estimates of crop stress. In particular, thermal imagery can be a sound approach for monitoring crop stress (Jackson et al. 1981; González-Dugo et al. 2014), and hence estimating water potential (Berni et al. 2009; Bellvert et al. 2016) or stomatal conductance (Inoue et al. 1990; Taconet et al. 1995; Jones 1999; Jones et al. 2002; Leinonen et al. 2006; Berni et al. 2009). More recent studies in vineyards showed that the Two Source Energy Balance model (Norman et al. 1995) was able to accurately estimate evapotranspiration, and its partitioning between soil evaporation and canopy transpiration, using thermal infrared measurements obtained either from in-situ radiometers (Kustas et al. 2018; Nieto et al. 2019a), airborne cameras (Nieto et al. 2019b) or satellite-borne sensors (Knipper et al. 2019, 2020). Indeed, Bellvert et al. (2020) showed that TSEB-derived transpiration showed a more robust relationship with midday stem water potential than bulk ET, as the latter is also influenced by the soil/substrate near-surface moisture and hence soil evaporation. Furthermore, Nieto et al. (2019a) hypothesized that from TSEB estimates of canopy latent heat fluxes and its derived aerodynamic resistances, it is possible to derive effective values of stomatal conductance from top-down approaches (Baldochi et al. 1991), similar to the techniques proposed by Jones et al. (2002), Leinonen et al. (2006), or Berni et al. (2009).

The majority of these previous studies using thermal remote sensing for crop water stress monitoring applied a normalization approach that related the radiometric temperature, or the estimated ET, to a reference value. This is the case of the widely used Crop Water Stress Index (CWSI), proposed by Jackson et al. (1981), which is computed as the ratio of actual ET over potential ET ( $CWSI = 1 - ET/ET_0$ ). This potential ET ( $ET_0$ ) is defined as the water usage (or evapotranspiration rate) of a well watered crop under the same physiological conditions as the given crop. The derivation of  $ET_0$  has been usually computed from the Penman–Monteith model, assuming a maximum (minimum) stomatal conductance (resistance). However, the “big-leaf” Penman–Monteith model estimates the fluxes as a single-source, not being able to physically separate crop transpiration from soil evaporation. Furthermore, the radiation transmission and the turbulent transport from canopy and interrow of a heterogeneous row crop such as trellised vineyards is likely to deviate from the physics of “big-leaf”

models (De Pury and Farquar 1997). On the other hand, the two-source energy combination model of Shuttleworth and Wallace (1985), which extended the Penman–Monteith energy combination approach to be applicable to sparse and heterogeneous crops, is hypothesized to be more suitable for evaluating the potential crop water needs and stress (Nieto et al. 2019a). With Shuttleworth–Wallace, there is the ability of estimating crop potential transpiration, and the capability of including the effect of the row structure in energy partitioning (Parry et al. 2019), as well as aerodynamic roughness variations with wind direction (Alfieri et al. 2019a).

Based on the previous observations, this study aims at evaluating different crop stress metrics derived from TSEB using in situ measurements for a 3-year experiment over a vineyard subject to different stress levels. The specific research questions that are addressed are:

1. What are the advantages and limitations of using stem/leaf water potential, stomatal conductance and canopy transpiration for tracking variations of root-zone soil moisture?
2. Is TSEB actual transpiration and/or stomatal conductance a better proxy for crop stress than bulk evapotranspiration?
3. Does the Shuttleworth–Wallace model provide any advantage over the Penman–Monteith model to evaluate crop potential needs, and hence CWSI?

## Materials and methods

The correlation and its significance ( $p$  value) will be the basis to evaluate the relationship between the different remote sensing crop stress metrics and the in situ physiological and root-zone soil moisture measurements. Moreover, TSEB transpiration and stomatal conductance will also be directly evaluated against their correspondent ground measurements.

### Crop stress metrics

Traditionally, the Crop Water Stress Index has been used to assess vegetation water stress, based on the relationship between actual and potential evapotranspiration (Jackson et al. 1981). In this study, we take advantage of the two source models to compute a series of alternative metrics in Eq. 1, under the assumption that canopy fluxes are more related to crop conditions than bulk fluxes:

$$CTSI = \frac{\lambda E_C}{\lambda E_{C,sw}} \quad (1a)$$

$$CSSI = \frac{g_s}{g_{st,0}} \tag{1b}$$

where CTSI stands for Crop Transpiration Stress Index and CSSI for Crop Stomatal Stress Index.  $\lambda E_C$  and  $\lambda E_{C,SW}$  are, respectively, actual TSEB and potential canopy latent heat fluxes computed with the Shuttleworth–Wallace model;  $g_s$  is the actual stomatal conductance, derived from TSEB, and  $g_{st,0}$  is the maximum stomatal conductance (see “Sensitivity of stomatal conductance to vapour pressure deficit” for its derivation).

In addition, since potential bulk latent heat flux can be defined in different forms, we evaluated different CWSI values, depending on whether the potential latent heat flux is computed from the Penman–Monteith equation, using a constant minimum stomatal resistance ( $CWSI-PM_{R_c, \min} = \lambda E / \lambda E_{PM_{R_c, \min}}$ , with  $R_c = 50 \text{ s m}^{-1}$ ) or a vapour pressure deficit (VPD) dependant stomatal resistance ( $CWSI-PM_{R_c, VPD} = \lambda E / \lambda E_{PM_{R_c, VPD}}$ ), as well as the potential latent heat flux computed from the Shuttleworth–Wallace model with VPD dependant stomatal resistance ( $CWSI-SW_{R_c, VPD} = \lambda E / \lambda E_{SW_{R_c, VPD}}$ ).

Finally, the fraction of actual ET to Allen et al. (1998) reference ET is also computed ( $f_{REF} = \frac{ET_{day}}{ET_{FAO56}}$ ) as a stress metric typically used in climate studies (Anderson et al. 2016). Note that all stress metrics are computed as a ratio, removing the term “1–” from the CWSI to ensure that stress indices have a lower limit of 0 for maximum stress (full stomatal closure), increasing to 1 for non-stressed vegetation (fully transpiring).

**Sensitivity of stomatal conductance to vapour pressure deficit**

Kustas et al. (2022) showed the advantages of accounting for the sensitivity of stomatal closure at higher VPD in canopies highly coupled with the atmosphere (Jarvis and McNaughton 1986). Based on the method proposed by Monteith (1995), Kustas et al. (2022) derived the stomatal parameters for the Leuning (1995) stomatal conductance model of Eq. 2:

$$g_{s,0} = \frac{g_m}{1 + VPD/D_0} \tag{2}$$

with  $g_m = 0.58 \text{ mol m}^{-2} \text{ s}^{-1}$  and  $D_0 = 15.85 \text{ mb}$ .

The canopy stomatal resistance ( $R_c$ ), dependent of VPD variations, is then computed from equation:

$$R_c = \frac{1}{g_{s,0} f_s f_g LAI} \tag{3}$$

where LAI is the leaf area index, defined as half of the total leaf area, and  $f_s$  is a factor representing the distribution of stomata in the leaf ( $f_s = 1$  for hypostomatous leaves and

$f_s = 2$  for amphistomatous leaves) and  $f_g$  is the fraction of LAI that is green and hence actively transpiring.

**Shuttleworth–Wallace model**

The two-source Shuttleworth–Wallace energy combination model (Shuttleworth and Wallace 1985) was specifically designed to account for evapotranspiration partitioning in sparse crops. Therefore, both the heat and water fluxes are separated into a soil and canopy layer, with a series of resistances set in series (Fig. 1).

Energy fluxes are, therefore, split into soil and canopy, considering the conservation of energy (Eq. 4):

$$R_n \approx H + \lambda E + G \tag{4a}$$

$$R_{n,S} \approx H_S + \lambda E_S + G \tag{4b}$$

$$R_{n,C} \approx H_C + \lambda E_C \tag{4c}$$

with  $R_n$  being the net radiation,  $H$  the sensible heat flux,  $\lambda E$  the latent heat flux or evapotranspiration, and  $G$  the soil heat flux (all fluxes are expressed in  $\text{W m}^{-2}$ ). The approximation in Eq. 4 reflects additional components of the energy balance that are usually neglected, such as heat advection, storage of energy in the canopy layer or energy for the fixation of  $\text{CO}_2$  (Hillel 1998; Baldocchi et al. 1991), which are not computed by the model.

Canopy latent heat flux (or transpiration) is computed from Eq. 5.

$$\lambda E_C = \frac{\Delta R_{n,C} + \rho_a c_p \frac{VPD_0}{R_x}}{\Delta + \gamma \left( 1 + \frac{R_c}{R_x} \right)} \tag{5}$$

where  $\rho_a$  is the air density;  $c_p$  the heat capacity of air,  $VPD_0$  is the air vapour pressure deficit at the canopy–air interface;  $R_x$  is the canopy boundary resistance to momentum, heat and vapour transport; and  $R_c$  is related to the leaf stomatal conductance  $g_s$  via Eq. 3

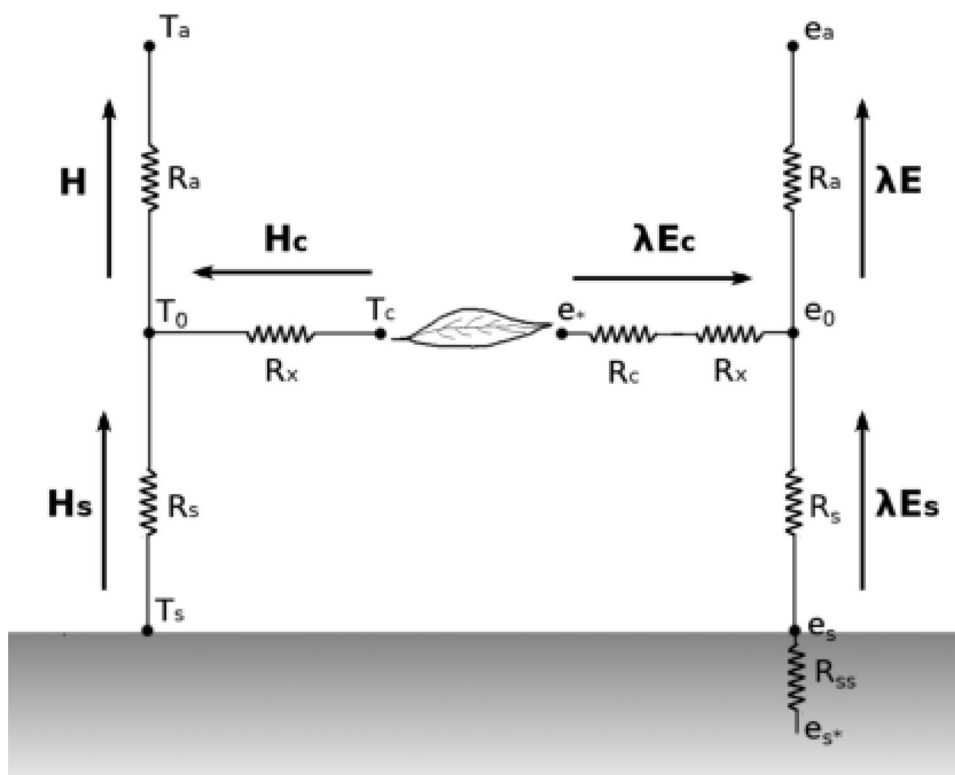
The vapor pressure deficit at the canopy–air interface ( $VPD_0$ ) is computed as (Shuttleworth and Wallace 1985)

$$VPD_0 = VPD + R_a \frac{\Delta (R_n - G) - (\Delta + \gamma) \lambda E}{\rho_a c_p} \tag{6}$$

where VPD is the measured atmospheric vapour pressure deficit,  $R_a$  is the aerodynamic resistance to turbulent transport,  $R_n$  is the surface net radiation,  $G$  is the soil heat flux, and  $\lambda E$  is the surface bulk (soil + canopy) latent heat flux, estimated as (Eq. 7):

$$\lambda E = C_c PM_C + C_s PM_S \tag{7}$$

**Fig. 1** Two-source energy balance scheme including the transport of both heat ( $H$ ) and water vapour ( $\lambda E$ ). Adapted from Shuttleworth and Wallace (1985)



$PM_C$  and  $PM_S$  are the estimates of an infinite deep canopy and bare soil latent heat fluxes, respectively, using the Penman–Monteith equation:

$$PM_C = \frac{\Delta(R_n - G) + \frac{\rho_a c_p VPD - \Delta R_x (R_{n,s} - G)}{R_a + R_x}}{\Delta + \gamma \left(1 + \frac{R_c}{R_a + R_x}\right)} \tag{8a}$$

$$PM_S = \frac{\Delta(R_n - G) + \frac{\rho_a c_p VPD - \Delta R_s R_{n,c}}{R_a + R_s}}{\Delta + \gamma \left(1 + \frac{R_{ss}}{R_a + R_s}\right)} \tag{8b}$$

where  $R_s$  is the soil boundary layer resistance to turbulent transport and  $R_{ss}$  is the near-surface soil resistance to vapour transport. The latter is set to a fixed value of  $R_{ss} = 2000 \text{ s m}^{-1}$  considering a rather dry soil surface, to be consistent with the definition of potential ET adopted with the Penman–Monteith approach.

**Priestley–Taylor two source energy balance model**

Remote sensing energy balance models, REBMs, rely on the ability of the radiometric information to estimate both net radiation (Liang et al. 2010) and sensible heat flux (Norman et al. 1995), whereas soil heat flux is usually estimated as a fraction of  $R_n$  (Liebethal and Foken 2007). Therefore, latent heat flux is retrieved as a residual of the remaining terms of

Eq. 4. In addition, REBMs need additional ancillary inputs, such as air temperature, wind speed and canopy height or roughness, to account for the efficiency in the turbulent transport of heat and water between the land surface and the overlying air (Raupach 1994; Shaw and Pereira 1982; Alfieri et al. 2019a). Specifically for TSEB, vegetation structure and density are also important for estimating wind and radiation extinction through the canopy layer affecting the radiation partitioning and turbulent transport of momentum, heat and water vapour in the canopy air space (Nieto et al. 2019a; Parry et al. 2019).

The key in TSEB models is the partition of sensible heat flux into the soil and canopy layers, which depends on the soil and canopy temperatures ( $T_s$  and  $T_c$ , respectively, left side of Fig. 1). Given the difficulty of obtaining the pure component temperatures, even with very high resolution data due to canopy gaps, Norman et al. (1995) found a solution to retrieve  $T_s$  and  $T_c$  using a single observation of the directional radiometric temperature  $T_{rad}(\theta)$  as this is the case for most of the remote sensing systems. Equation 9 decomposes the composite  $T_{rad}(\theta)$  temperature between its components  $T_s$  and  $T_c$ , assuming blackbody emission of thermal radiance:

$$\sigma T_{rad}^4(\theta) = f_c(\theta) \sigma T_c^4 + [1 - f_c(\theta)] \sigma T_s^4 \tag{9}$$

where  $f_c(\phi)$  is the fraction of vegetation observed by the sensor. Since Eq. 9 consists of two unknowns and only one

equation, an iterative process to find  $H_S$ ,  $T_S$ ,  $H_C$  and  $T_C$  is defined based upon an initial guess of potential canopy transpiration, and under the assumption that during daytime hours condensation for the soil/substrate should not occur. The initial canopy latent and sensible heat fluxes are estimated based on the Priestley and Taylor (1972) formulation for potential transpiration (Eq. 10) and Eq. 4.

$$\lambda E_C = \alpha_{PT} f_g \frac{\Delta}{\Delta + \gamma} R_{n,c} \quad (10a)$$

$$H_C = R_{n,c} - \lambda E_C \quad (10b)$$

where  $\alpha_{PT}$  is the Priestley–Taylor coefficient, initially set to 1.26,  $f_g$  is the fraction of vegetation that is green and hence capable of transpiring,  $\Delta$  is the slope of the saturation vapour pressure versus temperature,  $\gamma$  is the psychrometric constant.  $T_C$  is then computed by inverting the equation for turbulent transport of heat (see Norman et al. 1995) between the surface and the reference height above the surface)

With a first estimate of  $T_C$ , soil temperature is computed from Eq. 9 and then soil sensible and latent heat fluxes. At this stage, if soil latent heat flux results to be non-negative, a solution is found, otherwise canopy transpiration is reduced incrementally to avoid negative soil latent heat flux, until a realistic solution is found (no condensation occurring neither in the soil nor in the canopy in daytime). For more details the reader is addressed to the works of Norman et al. (1995) or Kustas and Norman (1999).

### Inversion of actual stomatal conductance

With an estimate of canopy fluxes and aerodynamic resistances, the effective conductance to water vapour diffusion exerted by all leaves in the canopy ( $R_c$ ,  $s \text{ m}^{-1}$ ) can then be estimated by the resistance network of Fig. 1 (Eq. 11):

$$R_c = \frac{\rho_a c_p (e_* - e_0)}{\lambda E_C \gamma} - R_x \quad (11)$$

where  $R_c$  represents the resistance to water diffusion through both the cuticle and stomata in the canopy ( $\text{m s}^{-1}$ ),  $e_*$  is the water vapour pressure in the leaf (kPa), which is assumed saturated at the leaf temperature  $T_C$  (K) (Farquhar and Sharkey 1982),  $R_x$  is the resistance to momentum and heat transport at the boundary layer of the canopy interface ( $\text{m s}^{-1}$ ), and  $e_0$  is the vapour pressure of the air at the canopy interface (kPa), which is related to the air water vapour pressure measured at the reference height  $e_a$  through Eq. 12 (Fig. 1):

$$e_0 = e_a + \frac{\lambda E \gamma R_a}{\rho_a c_p} \quad (12)$$

The conductance of the cuticle can be neglected with respect to the conductance of the stoma (Duursma et al. 2019). Therefore, the leaf effective stomatal conductance to  $\text{H}_2\text{O}$  can finally be computed by inverting Eq. 3.

Equation 11 shows that stomatal conductance depends on canopy transpiration ( $\lambda E_C$ ) and the canopy boundary layer resistances ( $R_x$ ). Furthermore,  $\lambda E_C$  depends at the same time on both soil  $R_s$  and canopy  $R_x$  resistances, from Eqs. A2 and A4 in Norman et al. (1995):

$$R_s = \frac{1}{c(T_S - T_A)^{1/3} + bU_S} \quad (13a)$$

$$R_x = \frac{C'}{\text{LAI}} \left( \frac{l_w}{U_{d+z_{oM}}} \right)^{1/2} \quad (13b)$$

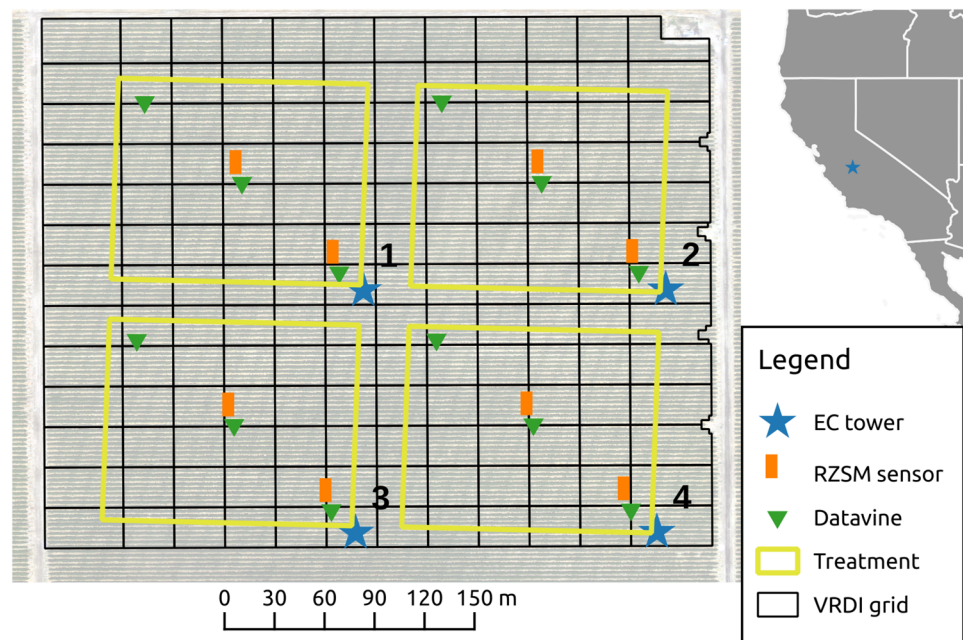
where  $d$  is the zero-plane displacement height,  $z_{oM}$  is the roughness length for momentum (all these magnitudes expressed in  $m$ ),  $U_S$  is the wind speed at the height  $z'$  above the soil surface, where the effect of the soil roughness is minimal ( $z' \approx 0.01\text{--}0.05 \text{ m}$ ). Coefficients  $b \approx 0.0012$  (Norman et al. 1995) and  $c \approx 0038 \text{ m s}^{-1} \text{ K}^{-1/3}$  (Kustas et al. 2016) depend on turbulent length scale in the canopy, soil-surface roughness and turbulence intensity in the canopy and are discussed in Sauer et al. (1995), Kondo and Ishida (1997) and Kustas et al. (2016).  $C'$  is assumed to be  $90 \text{ s}^{1/2} \text{ m}^{-1}$  Norman et al. (1995);  $l_w$  is the average leaf size ( $m$ ) and  $U_{d+z_{oM}}$  is the wind speed at the effective heat source/sink layer ( $d + z_{oM}$ ).

### Study site

The GRAPEX (Kustas et al. 2018) RIP720 experimental site, located in Madera county (CA, USA) is used in this study. The grapevine variety in this vineyard is Merlot, planted in 2010 and trellised in a bilateral cordon following an East–West row orientation. The spacing between rows is 3.35 m, with a plating interval of 1.52 m. The vineyard is on flat terrain at an elevation above mean sea level of approximately 60 m. Soil texture is sandy loam and interrow is covered by a cover crop that is planted in the Fall and is mowed once or twice in April/May the following year.

RIP720 includes a Variable Rate Deficit Irrigation infrastructure (Fig. 2) that allowed to impose several stress events in different irrigation sectors. For that reason, four Eddy Covariance (EC) towers were installed in April 2018 to track water and energy fluxes in those different sectors. In addition, soil moisture probes were installed along the typical flux footprint considering the prevailing winds (NW–SE).

**Fig. 2** RIP720 experimental vineyard with four Eddy Covariance towers (blue stars) placed to maximize fetch for the four different treatment sectors (yellow boxes). Orange rectangles represent the root-zone soil moisture (RZSM) probes and green triangles show the location of the data vines, where leaf water potential and gas exchange measurements were sampled. The black grid represents the variable-rate deficit irrigation (VRDI) network



### Flux data

The EC/energy balance systems were located approximately 20 m inside each vineyard at the south–east edge to have an adequate fetch for the prevailing winds from the north–west. A detailed description of the measurements and their post-processing is described by Alfieri et al. (2019b). Briefly the tower at each site is instrumented with an infrared gas analyzer (IRGASON, Campbell Scientific,<sup>1</sup> Logan, Utah) and a sonic anemometer (CSAT3, Campbell Scientific) co-located at 4 m agl to measure the concentrations of water and carbon dioxide and wind velocity, respectively. The full radiation budget was measured using a four-component net radiometer (CNR-1, Kipp and Zonen, Delft, Netherlands) mounted at 4.25 m agl. Air temperature and water vapor pressure at 4 m agl were measured using an aspirated shielded temperature and humidity probe (E+E Elektronik, Engerwitzdorf, Austria). Subsurface measurements include the soil heat flux measured via a cross-row transect of five plates (HFT-3, Radiation Energy Balance Systems, Bellevue, Washington) buried at a depth of 8 cm. Because of the frequent lack of energy balance closure using Eddy Covariance technique, the values of  $H$  and  $\lambda E$  observed were computed following the rationale described in Kustas et al. (2022). We derived the measured fluxes from an average (or ensemble) of three possible closure corrections, assigning all the residual error

to  $H$ , assigning all the residuals to  $\lambda E$ , and assigning the residual error proportionally to  $H$  and  $\lambda E$  by preserving the Bowen Ratio (i.e.,  $H/\lambda E$ ). Please see Kustas et al. (2022) and Bambach et al. (2022) for further details on the energy closure uncertainty and rationale behind various closure approaches.

### Physiological data

in situ physiological measurements were carried out in these four sectors since spring 2018. Sampling interval varied between years, with more frequent sampling during intensive observation campaigns, and coincident with Landsat overpasses under clear-skies. For each sector three vines were selected (Fig. 2) for sampling, and every time 3–5 adult leaves from the top half of the canopy and fully exposed to the sun were sampled. The stomatal conductance was measured on the abaxial side with a gas exchange analyzer (Li-Cor model 6400 or 6800; LI-COR Biosciences, Lincoln, NE). Immediately after the same leaves were excised to measure their leaf water potential with a pressure chamber (Scholander et al. 1965). In addition, 30–45 min before each sampling point, one leaf per vine was bagged using an opaque bag, and the stem water potential measured concurrent with the rest of leaf level measurements.

### Root zone soil moisture data

The root zone soil moisture (RZSM,  $\text{m}^3 \text{m}^{-3}$ ) estimates in the vine row were processed by Chen et al. (2022). The RZSM estimates were computed from vine-row sensors monitoring 5, 30, 60 and 90 cm depths at 15 cm distance and

<sup>1</sup> The use of trade, firm, or corporation names in this article is for the information and convenience of the reader. Such use does not constitute official endorsement or approval by the US Department of Agriculture or the Agricultural Research Service of any product or service to the exclusion of others that may be suitable.

5, 30, and 60 cm depths at 45 cm distance from the drip line centered along the vine row. The sensors used for measuring RZSM are model CS655 TDR probes from Campbell Scientific Inc., Logan, UT, USA. The daily RZSM was computed for the 30–60 cm layer along the vine rows as the average of sub-hourly soil moisture measurements from multiple 30 cm (in the southeast corners of each treatment, Fig. 2) or 40 cm (in the center location of each treatment, Fig. 2) depth, along with the sensors at 60 cm depth. This value is then averaged over a 24-h period within each irrigation treatment to obtain the daily RZSM used in this analysis. For more details in computing vine row RZSM, the reader is referred to Chen et al. (2022).

### TSEB implementation

To ensure a radiometric temperature encompassing both vine canopy and interrow surface temperatures the in situ measurements of upwelling longwave radiation from the pyrgeometer for deriving a radiative surface temperature were used. This allowed application of the TSEB model having the widest range of environmental conditions and acquisition times possible with a radiometric temperature similar to what might be observed by a satellite, such as Landsat. Therefore, TSEB-PT was run for every daytime hour, i.e., when shortwave irradiance is greater than  $100 \text{ W m}^{-2}$ , for the 3-year period (2018–2020) from mid-spring (DOY = 145) until the end of summer (DOY = 245). The hourly surface composite radiative temperature  $T_{\text{rad}}$  was extracted from the 4-component net radiometer, Eq. 14:

$$T_{\text{rad}} = \left( \frac{L^{\uparrow} - (1 - \epsilon_{\text{surf}})L^{\downarrow}}{\sigma \epsilon_{\text{surf}}} \right)^{1/4} \quad (14)$$

where  $L^{\uparrow}$  and  $L^{\downarrow}$  are the upwelling and downwelling measured longwave radiance,  $\sigma$  is the Stefan–Boltzmann constant, and  $\epsilon_{\text{surf}} = 0.99f_C + 0.94(1 - f_C)$  is the surface emissivity, assuming standard leaf and bare soil emissivity values of 0.99 and 0.94, respectively (Sobrino et al. 2005; Nieto et al. 2019a; Kustas et al. 2022). Additional inputs from the EC system were downwelling shortwave  $S^{\downarrow}$  irradiance, wind speed and direction, air temperature and humidity, and atmospheric pressure.

Estimates of daily LAI were obtained from training MODIS LAI (MCD15A3H) product and Landsat surface reflectance using the reference based approach (Gao et al. 2012) and adapted for vineyards by Kang et al. (2022). The homogeneous and high quality LAI retrievals from the MODIS LAI product were extracted to train Landsat and Sentinel-2 surface reflectance aggregated at the MODIS spatial resolution. The trained regression trees were then applied to a 30 m surface reflectance to produce

LAI. Daily LAI at 30 m Landsat resolution were then generated using the Savitzky–Golay moving window filter approach which smooths and fills the temporal gaps (Sun et al. 2017).

Canopy width  $w_c$ , canopy height  $h_c$ , and the height of the bottom of the canopy  $h_b$  were estimated from daily LAI using empirical curves fit with measured in situ values (Nieto et al. 2019b). The fraction of LAI that is green is set to a constant value of 1, considering that the study period only covers the vegetative grapevine stage.

Soil heat flux was estimated in TSEB-PT as a fraction of the net radiation at the soil  $R_{n,S}$  using the sinusoidal relationship by Santanello and Friedl (2003), with an amplitude of 0.35 for the fraction of  $R_{n,S}$ . In addition the specific radiative and turbulent environment in the grapevines is accounted for by considering the radiation partitioning between the vines and the soil model of Parry et al. (2019), the variation of aerodynamic roughness with wind direction by Alfieri et al. (2019a), and the turbulent transfer a rough soil/cover crop background by Kustas et al. (2016).

Daily latent heat flux ( $\lambda E_{\text{day}}$ ), and hence daily ET for computing the  $f_{\text{RET}}$  index, is estimated from instantaneous (i.e., hourly) metrics ( $\lambda E_i$ ) by assuming a constant ratio of latent heat flux and solar irradiance (Colaizzi et al. 2014; Cammalleri et al. 2014):

$$\lambda E_{\text{day}} = S_{\text{day}}^{\downarrow} \frac{\lambda E_i}{S_i^{\downarrow}}. \quad (15)$$

Temporal upscaling from instantaneous to daily values was considered only for two time periods: at 10:30, simulating a before-noon satellite thermal infrared observation, typical of Landsat or Sentinel-3 overpass, and 13:30, simulating an early afternoon satellite thermal infrared observation as the one planned for the Land Surface Temperature Monitoring (LSTM) Copernicus candidate mission (Koetz et al. 2018).

## Results

Figure 3 shows the daily timeseries measurements EC evapotranspiration (ET), satellite LAI, RZSM, as well as stem water potential and stomatal conductance around solar noon. The latter two are averages of all grapevines and leaves sampled per site between 10:00 and 14:00.

These plots show some stress events with differential RZSM and ET rates between sites. In addition, the LAI trends show a significant drop in spring 2019 for sites 2 and 3 caused by a concomitant herbicide treatment in these two sites. Finally it is worth noting the missing data of RZSM in 2018 for site 3 due to sensors not being installed until Fall of 2018.

**Fig. 3** Timeseries of observed daily actual ET ( $\text{mm day}^{-1}$ ), satellite Leaf Area Index, and root zone soil moisture (RZSM  $\text{m}^3 \text{m}^{-3}$ ), stem water potential ( $\Psi_{\text{stem}}$ , MPa), and leaf stomatal conductance ( $g_s$ ,  $\text{mol m}^{-2} \text{s}^{-1}$ )

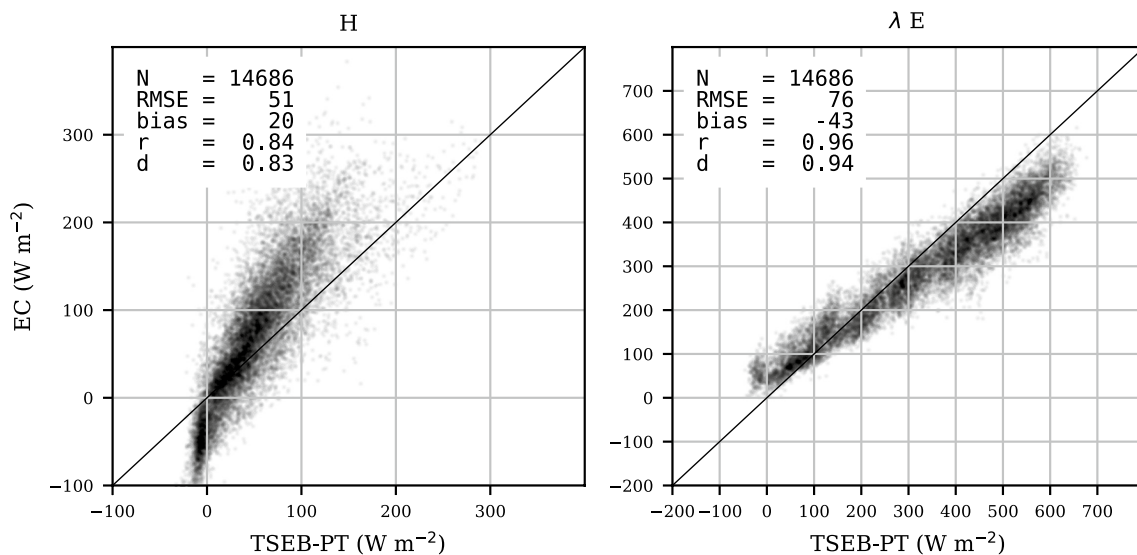
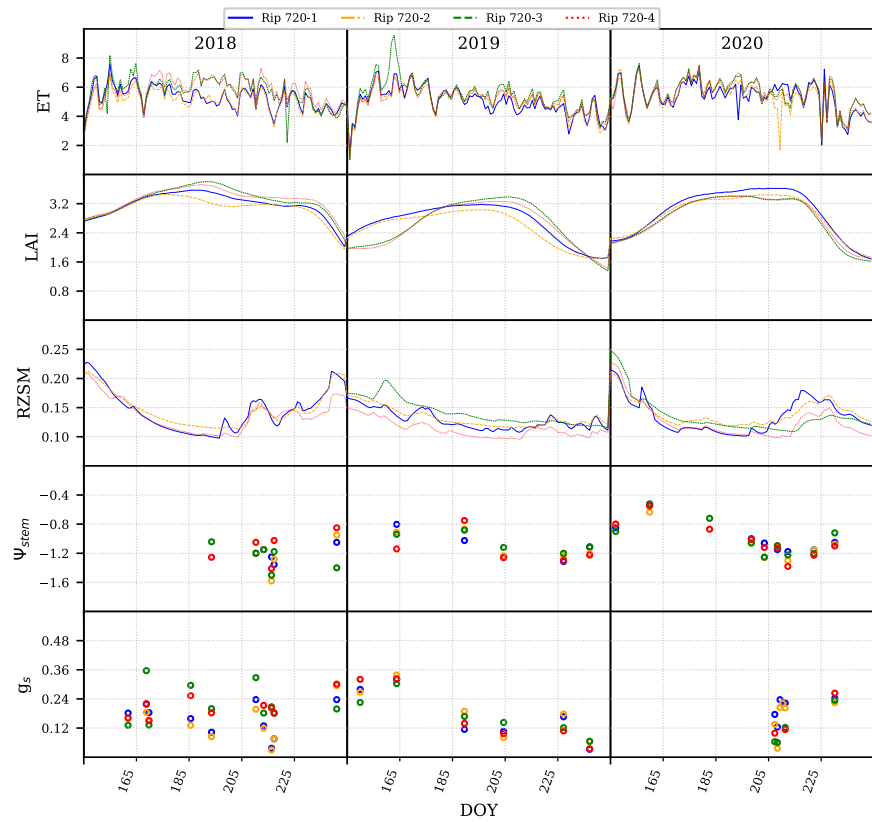


**Fig. 4** Predicted vs. observed scatterplot of hourly fluxes ( $\text{W m}^{-2}$ ) during daytime with TSEB initialized using the Priestley–Taylor potential transpiration. All four sites and all years 2018–2020 are plotted together.  $N$  is the number of cases used for validation, RMSE

is the root mean square error, bias is the mean bias computed as the observed minus the predicted,  $r$  is the Pearson correlation coefficient between the observed and the predicted and  $d$  is Willmott's index of agreement (Willmott 1982)



**Table 1** Site hourly error metrics ( $\text{W m}^{-2}$ ) for all valid daytime fluxes estimated for TSEB-PT.  $N$  is the number of cases used for validation, RMSE is the root mean square error, bias is the mean bias computed

Site	– $N$	Obs.		Bias		MAE		RMSE		$r$		$d$	
		$H$	$\lambda E$	$H$	$\lambda E$	$H$	$\lambda E$	$H$	$\lambda E$	$H$	$\lambda E$	$H$	$\lambda E$
Rip 720-1	3583	81	283	3	–34	34	54	44	68	0.87	0.96	0.89	0.94
Rip 720-2	3693	81	281	28	–54	42	71	56	86	0.84	0.96	0.78	0.92
Rip 720-3	3695	66	301	29	–45	43	62	54	75	0.91	0.97	0.78	0.95
Rip 720-4	3715	66	300	21	–40	38	63	48	75	0.93	0.96	0.81	0.95

as the observed minus de predicted,  $r$  is the Pearson correlation coefficient between the observed and the predicted and  $d$  is Willmott's index of agreement (Willmott 1982)

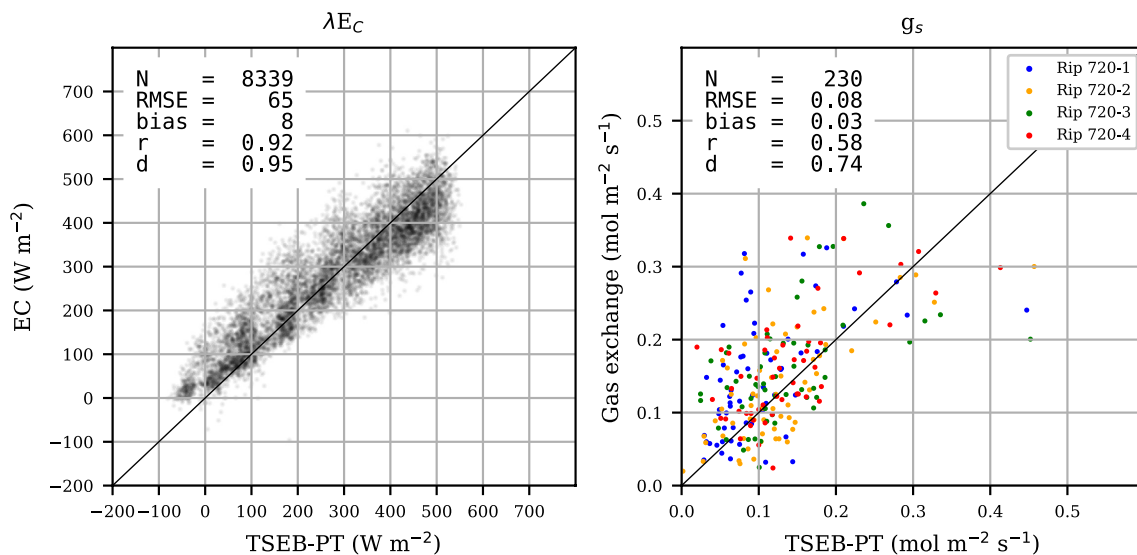


**Fig. 5** Predicted (TSEB-PT) vs. observed (EC or gas exchange measurements) scatterplot of daytime hourly left) canopy latent heat flux ( $\text{W m}^{-2}$ ) and right) stomatal conductance ( $\text{mol m}^{-2} \text{s}^{-1}$ ) with TSEB initialized using the Priestley–Taylor potential transpiration. All four sites are plotted together, with different colours in the case of stoma-

tal conductance.  $N$  is the number of cases used for validation, RMSE is the root mean square error, bias is the mean bias computed as the observed minus the predicted,  $r$  is the Pearson correlation coefficient between the observed and the predicted and  $d$  is Willmott's index of agreement (Willmott 1982)

## Bulk surface fluxes

Figure 4 shows the observed vs. predicted scatterplots of hourly daytime ( $S^{\downarrow} \geq 100 \text{ W m}^{-2}$ ) sensible and latent heat fluxes for TSEB-PT for all sites and 3 years studied between DOY 145 and 245. Table 1 lists the error statistics for each sector separately.

These results show the consistency of TSEB-PT in estimating both heat and water vapor fluxes with errors within the expected range ( $50\text{--}100 \text{ W m}^{-2}$ ) and strong correlation between the observed and the predicted values. Nevertheless, Table 1 shows a lower magnitude of mean bias and RMSE for RIP720-1 for both  $H$  ( $3 \text{ W m}^{-2}$  bias and  $44 \text{ W m}^{-2}$  RMSE) and  $\lambda E$  ( $-34 \text{ W m}^{-2}$  bias and  $68 \text{ W m}^{-2}$  RMSE).

## Canopy fluxes

The performance of TSEB-PT in estimating the hourly daytime canopy fluxes is depicted in Fig. 5. This figure shows the validation of canopy latent heat flux (or transpiration) using as measured values the flux partitioning ensemble as estimated by Thomas et al. (2008) Modified Relaxed Eddy Accumulation method and the Zahn et al. (2022) Conditional Eddy Covariance analysis. In addition this figure also shows the validation of the stomatal conductance measured in situ versus the estimated effective stomatal conductance from TSEB, using Eqs. 11 and 12.

The errors on hourly daytime canopy latent heat flux shown in Fig. 5 are in the same magnitude range than with the hourly daytime bulk latent heat flux

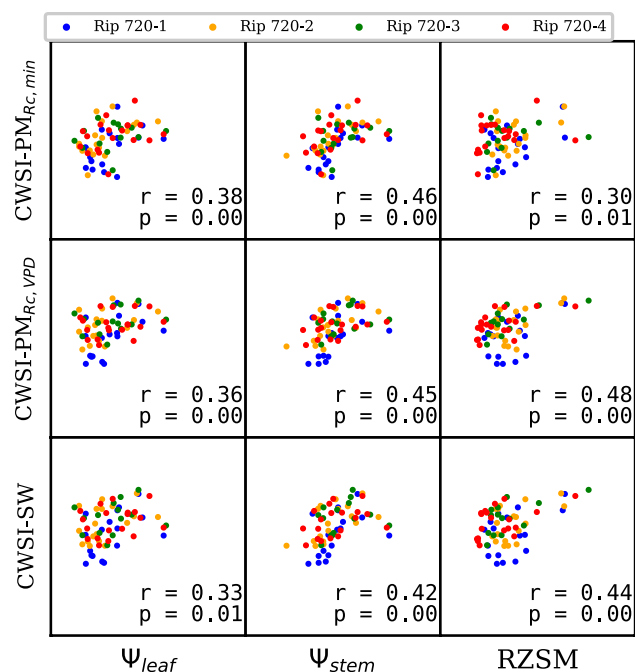


**Fig. 6** Relationship between CWSI values derived with TSEB-PT at 10:30 and (left) leaf water potential, (center) stem water potential and (right) root-zone soil moisture content. Potential  $\lambda E$  was calculated from (up) Penman–Monteith model using a constant minimum stomatal resistance, (middle) Penman–Monteith model using a VPD dependent minimum stomatal resistance, and (bottom) Shuttleworth–Wallace model using a VPD dependent minimum stomatal resistance. Each plot shows the Pearson correlation coefficient between the  $x$ - and  $y$ -metrics and its  $p$  value. Ticks and their labels are removed from the plots to enhance visibility

(RMSE =  $65 \text{ W m}^{-2}$ ), showing the ability of TSEB-PT model in ET partitioning between soil evaporation and canopy transpiration, despite of the simplicity of the Priestley–Taylor approach in defining a first-guess potential transpiration. This is confirmed when looking at the evaluation of the stomatal conductance on the right of Fig. 5. Considering the uncertainties in up(downscaling) in situ sunlit stomatal conductance (TSEB conductance), both metrics agreed reasonably well with minimum bias ( $0.03 \text{ mol m}^{-2} \text{ s}^{-2}$ ), low RMSE ( $0.08 \text{ mol m}^{-2} \text{ s}^{-2}$ ) and a correlation between the measured and the predicted of 0.58.

### Stress metrics

Daily stress metrics are computed both before noon (10:30) and early afternoon (13:30) for the different version of CWSI. Considering that in situ measurements are sometimes not concurrent and also due to soil moisture sensor failures, these correlations are only shown for the

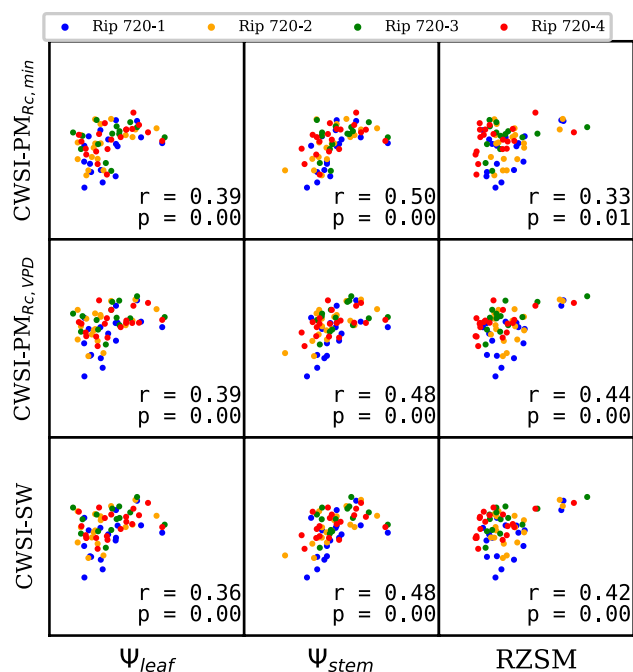


**Fig. 7** Relationship between CWSI values derived with TSEB-PT at 13:30 and (left) leaf water potential, (center) stem water potential and (right) root-zone soil moisture content. Potential  $\lambda E$  was calculated from (up) Penman–Monteith model using a constant minimum stomatal resistance, (middle) Penman–Monteith model using a VPD dependent minimum stomatal resistance, and (bottom) Shuttleworth–Wallace model using a VPD dependent minimum stomatal resistance. Each plot shows the Pearson correlation coefficient between the  $x$ - and  $y$ -metrics and its  $p$  value. Ticks and their labels are removed from the plots to enhance visibility

68 cases, where measurements are coincident, in order to make for a more fair inter-comparison between metrics. These results are shown in Figs. 6 and 7.

The alternative stress metrics  $f_{REF}$ , CTSI and CSSI, are also compared to near noon average water potentials (both leaf and stem) as well as daily Root Zone Soil Moisture in Fig. 8 for the 10:30 observation and Fig. 9 for the early afternoon (13:30) observation.

Results of Figs. 8 and 9 show that the highest correlation occurs between the CSSI (related to the stomatal conductance estimates) and the root zone soil moisture, with a correlation of 0.53 and 0.61 when using observations before noon and in the early afternoon, respectively. It is also worth noting that when evaluating the different versions of CWSI, considering a stomatal dependent closure on VPD (either within the Penman–Monteith or the Shuttleworth–Wallace model) yields better relationship with the in situ root zone soil moisture than when the stomatal resistance is set constant. On the other hand, CWSI-PM<sub>Rc,min</sub> shows slightly better correlation with water potentials than the other two CWSI versions.

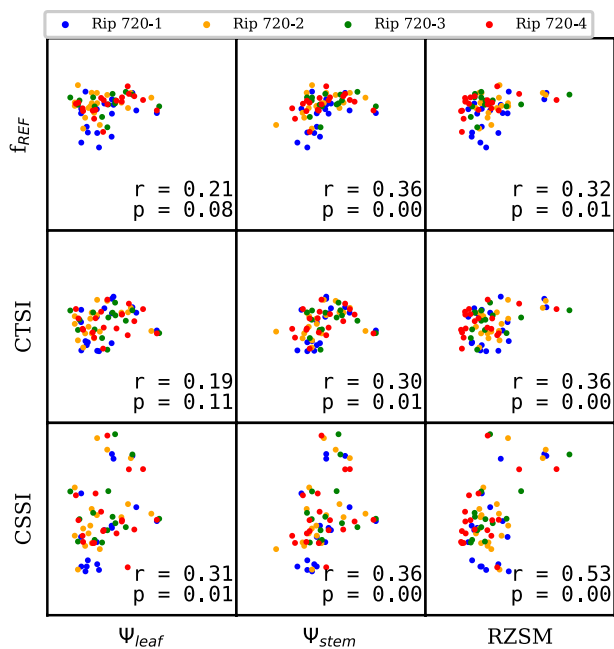


**Fig. 8** Relationship between the TSEB-PT alternative crop stress metrics at 10:30 and (left) leaf water potential, (center) stem water potential and (right) root zone soil moisture content. Each plot shows the Pearson correlation coefficient between the  $x$ - and  $y$ -metrics and its  $p$  value. Ticks and their labels are removed from the plots to enhance visibility

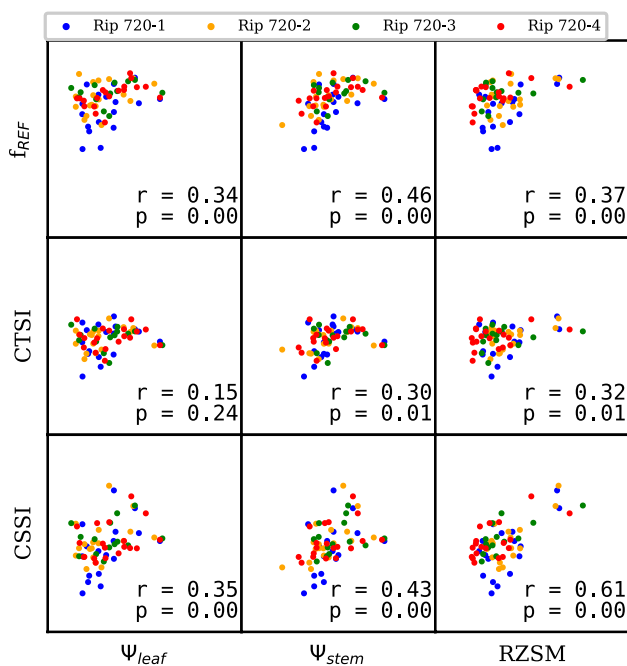


**Fig. 9** Relationship between the TSEB-PT alternative crop stress metrics at 13:30 and (left) leaf water potential, (center) stem water potential and (right) root zone soil moisture content. Each plot shows the Pearson correlation coefficient between the  $x$ - and  $y$ -metrics and its  $p$  value. Ticks and their labels are removed from the plots to enhance visibility

## Discussion

Results of this study indicate that TSEB is capable of providing reliable estimates of soil/substrate and canopy energy and canopy fluxes in a vineyard subject to different water stress events. The range of errors when validating hourly sensible and latent heat fluxes (Fig. 4) are within the expected uncertainty of the models and measurements ( $50\text{--}100\text{ W m}^{-2}$ ), with RMSE values of 51 and  $76\text{ W m}^{-2}$  for sensible and latent heat fluxes, respectively. Other studies showed a similar range of errors in other locations (Nieto et al. 2019a) and under a larger evaporative demand (Kustas et al. 2022).

However, it must be also considered that in situ measurements of energy and water fluxes are not free of uncertainties, such as the evidence of a lack of closure in the energy balance of the Eddy Covariance Systems (Bambach et al. 2022).

*Is TSEB actual transpiration and/or stomatal conductance a better proxy for crop stress than bulk evapotranspiration?* This study made a significant step in the assessment of TSEB model by evaluating for the first time (to the authors' knowledge) the performance of the model in deriving the stomatal conductance, by assessing these estimates against in situ gas exchange measurements. Results of Fig. 5 are promising, as TSEB-PT produced minimum bias ( $0.03\text{ mol m}^{-2}\text{ s}^{-1}$ ) and low RMSE ( $0.08\text{ mol m}^{-2}\text{ s}^{-1}$ ), although the explained variability of  $g_s$  by TSEB is marginal ( $r = 0.58$ ) compared to the model performance in estimating ET or the canopy latent heat fluxes. In this regard, it is worth noting that upscaling in situ  $g_s$  (bottom-up approach) is challenging in cases, where a significant spatial variability of conductance/vegetation stress exists (Baldochi et al. 1991), while these measurements are typically performed on a small sample of leaves within the canopy and in most case only on the sunlit fraction (such as in this study). On the other hand, the (top-down) inversion of the resistance scheme of Fig. 1 produced a rather effective leaf stomatal conductance, as an integrated value of the conductances of all sunlit and shaded leaves in the canopy. Finally, several other downscaling methods, or top-down approaches, have attempted to estimate canopy conductance to provide cost-effective and spatially distributed fields of  $g_s$  by remote sensing data (Taconet et al. 1995; Jones 1999; Leinonen et al. 2006; Berni et al. 2009), but most of these approaches are based on a single-source or “big-leaf” models based on the Penman–Monteith equation, and therefore, they usually consist in a bulk canopy conductance (Baldochi et al. 1991). Recently, Wehr and Saleska (2021) proposed a top-down approach that is based on the flux-gradient equation and includes as well a leaf boundary layer resistance, instead

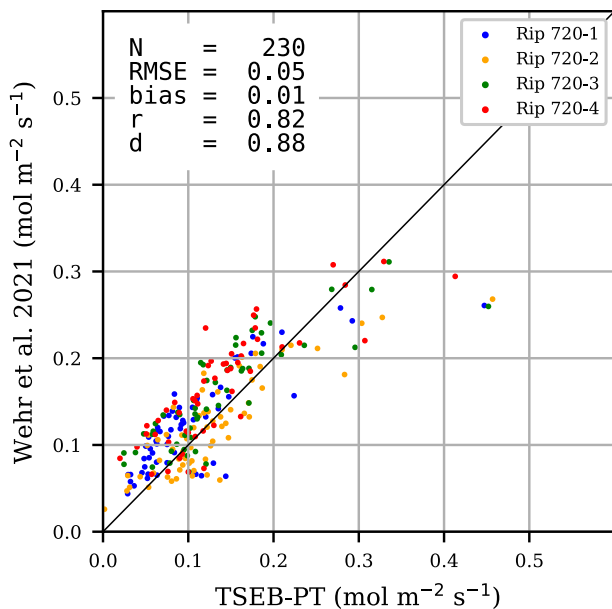


**Fig. 10** Intercomparison between  $g_s$  retrieved from TSEB-PT and using Wehr and Saleska (2021) model for the same cases shown in Fig. 5b

of inverting Penman–Monteith equation. Figure 10 shows the comparison between TSEB-PT derived  $g_s$  and the stomata conductance inverted by Wehr and Saleska (2021) approach, in which the in situ canopy EC flux data were used only for the cases with available in situ  $g_s$  measurements. Both estimates agree well each other and hence yield more similar values compared to the results using in situ measurements, as shown in Fig. 5b. It is noteworthy that while the in situ gas exchange measurements correspond to 3–5 leaves that are considered representative of the whole sunlit fraction of the canopy, both TSEB-PT and Wehr and Saleska (2021) derive effective values of  $g_s$  by downscaling canopy fluxes and, therefore, represent a stomatal conductance representative of a leaf under mean environmental conditions. Thus, discrepancies between leaf level observations of  $g_s$  at full light and estimations of a leaf theoretically exposed to mean light conditions is expected.

Finally, the correlations between the different TSEB stress metrics and the in situ measurements (Figs. 6, 7, 8 and 9) showed that the best performing pair was the use of the actual to maximum leaf stomatal conductance ratio (CSSI) and the root zone soil moisture, with a correlation of 0.53 and 0.61 depending on whether a before noon or an early afternoon is used for the remote sensing acquisition, outperforming even the use of the actual to potential transpiration ratio (CTSI).

*Does the Shuttleworth–Wallace model provide any advantage over the Penman–Monteith model to evaluate*

*crop potential needs, and hence CWSI?* The different CWSI methods, either using the Penman–Monteith or Shuttleworth–Wallace, tend to yield better results than CTSI (computed from the Shuttleworth–Wallace model) despite CWSI using ET, while CTSI uses only information on the canopy transpiration. This is somewhat opposite to what was observed by Bellvert et al. (2020), in which they showed a more robust behaviour between TSEB transpiration and stem water potential than using TSEB ET. One of the plausible explanations for this poorer performance of CTSI can be due to the definition of the term “potential”. Usually the potential ET is defined as a surface with a rather dry top-soil but with plenty of water at the root-zone, or simply a “big-leaf” canopy. However, it is worth noting that the soil surface moisture affects not only the bulk ET (via soil evaporation) but also the evaporative demand by the canopy, and hence the transpiration rate. A dry and exposed soil surface will release hot and dry air parcels towards the canopy, increasing the temperature and VPD at the canopy–air interface, and hence increasing its evaporative demand (e.g., Kustas and Norman 1999). On the contrary, a wet soil surface will enhance the convection of cool and moist air parcels towards the canopy, and thus reducing its evaporative demand. This effect is well accounted for in the Shuttleworth–Wallace model, as it is a layered model with resistances in series through Eq. 12. Therefore, for any given crop phenological status, root-zone soil moisture and atmospheric forcing, the transpiration rate at the canopy would vary depending on the surface soil moisture, and hence the calculation of crop potential needs should ideally account for this issue.

*Advantages and limitations of using stem/leaf water potential, stomatal conductance and canopy transpiration for tracking variations of root-zone soil moisture* Water potentials tend to show a poorer performance to the TSEB stress indices, particularly for the case of the leaf water potential (Figs. 6, 7, 8 and 9). Only when using the standard CWSI, computed with the Penman–Monteith model with a fixed canopy resistance of  $50 \text{ s m}^{-1}$ , the stem water potential tends to show slightly better performance than with the root-zone soil moisture. Several authors have already pointed out the limitations of leaf or stem water potential in robustly tracking water stress (Flexas et al. 2004; Jones 2004; García-Tejera et al. 2021). One of these limitations are related to the canopy growth, and in the case of vineyards, their canopy management interventions (e.g., pruning, leafing, hedging), which modifies the root to leaf area ratio and hence the hydraulic conductivity of the soil–plant–atmosphere continuum. Indeed, some studies that related remote sensing metrics to water potential usually found that these empirical relations are significantly different among phenological stages (Bellvert et al. 2015, 2016). Furthermore, the severity and length of the water stress events vary depending on the growth and canopy environment as well as the production

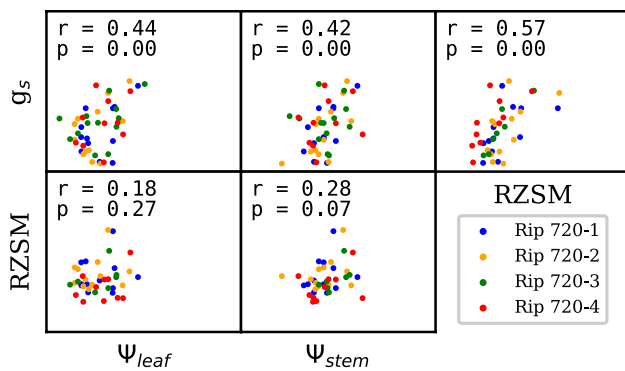


**Fig. 11** Relationship between in situ measurements of stomatal conductance ( $g_s$ ), leaf water potential ( $\Psi_{leaf}$ ), stem water potential ( $\Psi_{stem}$ ) and root zone soil moisture (RZSM). The correlation between leaf and stem water potential is 0.86 ( $p$  value  $< 0.01$ ), (not shown as a scatterplot). All plots represent the same number of cases ( $N = 47$ ) and each plot shows the Pearson correlation coefficient between the  $x$ - and  $y$ -metrics and its  $p$  value. Ticks and their labels are removed from the plots to enhance visibility

objective, and the physiological response of plants and vine varieties to the various deficit irrigation strategies adds up to the difficulty of interpreting the same value of midday  $\Psi$  across different scenarios. Stomatal conductance ( $g_s$ ) provides an added value to the water potential as it links the fluxes of water and  $CO_2$  in plants (Farquhar and Sharkey 1982), and consequently between transpiration and photosynthesis (Jarvis 1976; Escalona et al. 1999). Therefore,  $g_s$  affects processes related to the crop physiology, but as well as on the atmosphere chemistry, the water cycle and the climate at different scales (Baldocchi et al. 1991). The value of  $g_s$  is, therefore, a key factor not only used for assessing vegetation stress, but also in modelling carbon uptake and crop productivity (Escalona et al. 1999; Jones et al. 2002).

Despite the fact that several studies have proposed  $\Psi$  thresholds as the triggering event when applying irrigation (Girona et al. 2006; van Leeuwen et al. 2009; Intrigliolo et al. 2016; Merli et al. 2016), and that may be a good strategy for the scenarios, where the thresholds were established, the results of this study agree better with other studies that suggest using  $g_s$  instead (Jones 1999; Flexas et al. 2004). Indeed, the correlation of the in situ near noon measurements of  $g_s$ , water potentials and root-zone soil moisture are depicted in Fig. 11, showing that the strongest correlation is between the observed  $g_s$  and root-zone soil moisture ( $r = 0.57$ ), while the correlation between water potentials and RZSM are lower and non-significant ( $p$  value  $> 0.05$ ).

**Timing of thermal measurements** One of the advantages of using continuous in situ thermal infrared measurements is that they permit model benchmarking at different times of the day, regardless of the cloud coverage conditions. Results of Figs. 6 and 8, in which the TSEB metrics were obtained from an observation before noon (10:30), together with

Figs. 7 and 9 shows that an observation earlier in the afternoon (13:30) tends to better explain the stress conditions, with higher correlation between the stress indices and the in situ measurements. This is particularly evident with the significant increase of correlation between CSSI and RZSM, from 0.53 (Fig. 8) to 0.61 (Fig. 8). These results suggests that a thermal infrared observation around 13:30 would provide better information than at 10:30, when the overpass of most of the satellite thermal missions (e.g., Landsat) occur. This issue would support the mission requirements of the Sentinel Candidate Mission LSTM (Land Surface Temperature Monitoring) described in Koetz et al. (2021). LSTM will carry onboard a high resolution thermal infrared sensor (30–50 m resolution) with a revisit frequency of 1–3 days. It also verifies the advantage of a satellite system, such as ECOSTRESS sensor, currently on the International Space Station, occasionally providing an afternoon land surface temperature over the same area (Anderson et al. 2021). However, as shown by Kustas et al. (2022), observations in the afternoon are expected to be affected by advection of dry and hot air masses from dry areas into irrigated fields, posing a challenge in modeling sensible and latent heat fluxes and hence stress indices.

## Conclusions

This study evaluated whether the TSEB model was able to explain water stress conditions, by relating canopy and leaf metrics, such as evapotranspiration, transpiration, or stomatal conductance, with measurements collected in an irrigated vineyard in California subject to several stress events. Results confirmed the ability of TSEB in modelling latent heat fluxes both bulk and canopy, but moved one step forward and showed as well the potential of TSEB in retrieving effective values of leaf stomatal conductance.

From the metrics computed, the best performing stress index was the ratio of actual over maximum stomatal conductance (named in this study as Crop Stomatal Stress Index), which was able to explain the spatio-temporal variability of root-zone soil moisture and, to a lesser degree, the leaf and stem water potentials. Regarding the water potentials, the results confirmed the limitation of this metric, an issue that has been previously pointed out. Therefore, irrigation schedule practices should consider the limitations of using the water potential as the reference index for triggering and/or quantifying irrigation, especially since stomatal conductance seem to be better correlated to root-zone soil moisture content than leaf or stem water potentials. The TSEB crop stress metrics showed a better correlation with the in situ measurements when the thermal infrared acquisition was taken early in the afternoon, confirming the goal overpass time of LSTM mission. However, it is worth noting

that this study does not aim to evaluate errors in daily ET daily at different overpass times. This is a different topic that has already been addressed (e.g., Nassar et al. 2021), which still needs further investigation.

Finally, it is worth emphasizing that the degree of stomatal closure is the plant's way at preventing plant desiccation while maximizing the passage of CO<sub>2</sub>. Therefore, it is also a crucial variable for modelling/predicting plant productivity and hence yield. However, the relationship between transpiration and assimilation rates is not linear (Farquhar and Sharkey 1982), which makes the modelling of CO<sub>2</sub> challenging. Therefore, in a future study it is planned to integrate the TSEB conductance retrievals into an assimilation model to perform joint predictions of heat, water and CO<sub>2</sub> fluxes.

**Acknowledgements** Funding and logistical support for the GRAPEX project were provided by E. & J. Gallo Winery and from the NASA Applied Sciences-Water Resources Program (Grant no. NNH17AE39I). This research was also supported in part by the U.S. Department of Agriculture, Agricultural Research Service. In addition, we thank the staff of Viticulture, Chemistry and Enology Division of E. & J. Gallo Winery for the collection and processing of field data and the cooperation of the vineyard management staff for logistical support and coordinating field operations with the GRAPEX team.

**Funding** Open Access funding provided thanks to the CRUE-CSIC agreement with Springer Nature.

## Declarations

**Conflict of interest** On behalf of all authors, the corresponding author states that there is no conflict of interest.

**Open Access** This article is licensed under a Creative Commons Attribution 4.0 International License, which permits use, sharing, adaptation, distribution and reproduction in any medium or format, as long as you give appropriate credit to the original author(s) and the source, provide a link to the Creative Commons licence, and indicate if changes were made. The images or other third party material in this article are included in the article's Creative Commons licence, unless indicated otherwise in a credit line to the material. If material is not included in the article's Creative Commons licence and your intended use is not permitted by statutory regulation or exceeds the permitted use, you will need to obtain permission directly from the copyright holder. To view a copy of this licence, visit <http://creativecommons.org/licenses/by/4.0/>.

## References


- Alfieri JG, Kustas WP, Nieto H et al (2019a) Influence of wind direction on the surface roughness of vineyards. *Irrig Sci* 37(3):359–373. <https://doi.org/10.1007/s00271-018-0610-z>
- Alfieri JG, Kustas WP, Prueger JH et al (2019b) A multi-year inter-comparison of micrometeorological observations at adjacent vineyards in California's Central Valley during GRAPEX. *Irrig Sci* 37(3):345–357. <https://doi.org/10.1007/s00271-018-0599-3>
- Allen R, Pereira L, Raes D et al (1998) Crop evapotranspiration—guidelines for computing crop water requirements—FAO irrigation and drainage paper 56. Technical report, FAO—Food and Agriculture Organization of the United Nations
- Anderson MC, Zolin CA, Sentelhas PC et al (2016) The Evaporative Stress Index as an indicator of agricultural drought in Brazil: an assessment based on crop yield impacts. *Remote Sens Environ* 174:82–99. <https://doi.org/10.1016/j.rse.2015.11.034>
- Anderson MC, Yang Y, Xue J et al (2021) Interoperability of ECOSTRESS and Landsat for mapping evapotranspiration time series at sub-field scales. *Remote Sens Environ* 252(112):189. <https://doi.org/10.1016/j.rse.2020.112189>
- Baldocchi DD, Luxmoore RJ, Hatfield JL (1991) Discerning the forest from the trees: an essay on scaling canopy stomatal conductance. *Agric For Meteorol* 54(2):197–226. [https://doi.org/10.1016/0168-1923\(91\)90006-C](https://doi.org/10.1016/0168-1923(91)90006-C)
- Bambach N, Alfieri J, Prueger J et al (2022) Canopy level evapotranspiration uncertainty: the impact of different data processing and energy budget closure methods. *Irrig Sci* (in review)
- Bellvert J, Marsal J, Girona J et al (2015) Seasonal evolution of crop water stress index in grapevine varieties determined with high-resolution remote sensing thermal imagery. *Irrig Sci* 33(2):81–93. <https://doi.org/10.1007/s00271-014-0456-y>
- Bellvert J, Zarco-Tejada P, Marsal J et al (2016) Vineyard irrigation scheduling based on airborne thermal imagery and water potential thresholds. *Aust J Grape Wine Res* 22(2):307–315. <https://doi.org/10.1111/ajgw.12173>
- Bellvert J, Jofre-Čekalović C, Pelechá A et al (2020) Feasibility of using the Two-Source Energy Balance model (TSEB) with Sentinel-2 and Sentinel-3 images to analyze the spatio-temporal variability of vine water status in a vineyard. *Remote Sens*. <https://doi.org/10.3390/rs12142299>
- Berni J, Zarco-Tejada P, Sepulcre-Cantó G et al (2009) Mapping canopy conductance and CWSI in olive orchards using high resolution thermal remote sensing imagery. *Remote Sens Environ* 113(11):2380–2388. <https://doi.org/10.1016/j.rse.2009.06.018>
- Bravdo B, Hepner Y, Loinger C et al (1985) Effect of irrigation and crop level on growth, yield and wine quality of cabernet sauvignon. *Am J Enol Vitic* 36(2):132–139
- Cammalleri C, Anderson MC, Kustas WP (2014) Upscaling of evapotranspiration fluxes from instantaneous to daytime scales for thermal remote sensing applications. *Hydrol Earth Syst Sci* 18(5):1885–1894. <https://doi.org/10.5194/hess-18-1885-2014>
- Chen F, Lei F, Knipper K et al (2022) Application of the vineyard data assimilation (VIDA) system to vineyard root-zone soil moisture monitoring in the California Central Valley. *Irrig Sci* (in review)
- Cifre J, Bota J, Escalona J et al (2005) Physiological tools for irrigation scheduling in grapevine (*Vitis vinifera* L.): an open gate to improve water-use efficiency? *Agric Ecosyst Environ* 106(2):159–170. <https://doi.org/10.1016/j.agee.2004.10.005>
- Colaizzi P, Agam N, Tolck J et al (2014) Two-source energy balance model to calculate E, T, and ET: comparison of Priestley–Taylor and Penman–Monteith formulations and two time scaling methods. *Trans ASABE* 57(2):479–498. <https://doi.org/10.13031/trans.57.10423>
- De Pury DGG, Farquhar GD (1997) Simple scaling of photosynthesis from leaves to canopies without the errors of big-leaf models. *Plant Cell Environ* 20(5):537–557. <https://doi.org/10.1111/j.1365-3040.1997.00094.x>
- Duursma RA, Blackman CJ, López R et al (2019) On the minimum leaf conductance: its role in models of plant water use, and ecological and environmental controls. *New Phytol* 221(2):693–705. <https://doi.org/10.1111/nph.15395>
- Eastham J, Gray SA (1998) A preliminary evaluation of the suitability of sap flow sensors for use in scheduling vineyard irrigation. *Am J Enol Vitic* 49(2):171–176
- Escalona JM, Flexas J, Medrano H (1999) Stomatal and non-stomatal limitations of photosynthesis under water stress in field-grown

- grapevines. *Funct Plant Biol* 26(5):421–433. <https://doi.org/10.1071/PP99019>
- Farquhar GD, Sharkey TD (1982) Stomatal conductance and photosynthesis. *Annu Rev Plant Physiol* 33(1):317–345
- Flexas J, Bota J, Cifre J et al (2004) Understanding down-regulation of photosynthesis under water stress: future prospects and searching for physiological tools for irrigation management. *Ann Appl Biol* 144(3):273–283. <https://doi.org/10.1111/j.1744-7348.2004.tb00343.x>
- Gao F, Kustas WP, Anderson MC (2012) A data mining approach for sharpening thermal satellite imagery over land. *Remote Sens* 4(11):3287–3319. <https://doi.org/10.3390/rs4113287>
- García-Tejera O, López-Bernal A, Orgaz F et al (2021) The pitfalls of water potential for irrigation scheduling. *Agric Water Manag* 243(106):522. <https://doi.org/10.1016/j.agwat.2020.106522>
- Ginestar C, Eastham J, Gray S et al (1998) Use of sap-flow sensors to schedule vineyard irrigation. I. Effects of post-veraison water deficits on water relations, vine growth, and yield of shiraz grapevines. *Am J Enol Vitic* 49(4):413–420
- Girona J, Mata M, del Campo J, Arbonés A et al (2006) The use of midday leaf water potential for scheduling deficit irrigation in vineyards. *Irrig Sci* 24(2):115–127. <https://doi.org/10.1007/s00271-005-0015-7>
- González-Dugo V, Zarco-Tejada P, Fereres E (2014) Applicability and limitations of using the crop water stress index as an indicator of water deficits in citrus orchards. *Agric For Meteorol* 198–199:94–104. <https://doi.org/10.1016/j.agrformet.2014.08.003>
- Hillel D (1998) *Environmental soil physics*. Academic Press, Cambridge
- Inoue Y, Kimball BA, Jackson RD et al (1990) Remote estimation of leaf transpiration rate and stomatal resistance based on infrared thermometry. *Agric For Meteorol* 51(1):21–33. [https://doi.org/10.1016/0168-1923\(90\)90039-9](https://doi.org/10.1016/0168-1923(90)90039-9)
- Intrigliolo D, Lizama V, García-Esparza M et al (2016) Effects of post-veraison irrigation regime on Cabernet Sauvignon grapevines in Valencia, Spain: yield and grape composition. *Agric Water Manag* 170:110–119. <https://doi.org/10.1016/j.agwat.2015.10.020>
- Jackson RD, Idso SB, Reginato RJ et al (1981) Canopy temperature as a crop water stress indicator. *Water Resour Res* 17(4):1133–1138. <https://doi.org/10.1029/WR017i004p01133>
- Jarvis PG (1976) The interpretation of the variations in leaf water potential and stomatal conductance found in canopies in the field. *Philos Trans R Soc Lond B Biol Sci* 273(927):593–610. <https://doi.org/10.1098/rstb.1976.0035>
- Jarvis P, McNaughton K (1986) Stomatal control of transpiration: scaling up from leaf to region. In: *Advances in ecological research*, vol 15. Academic Press, Cambridge, pp 1–49. [https://doi.org/10.1016/S0065-2504\(08\)60119-1](https://doi.org/10.1016/S0065-2504(08)60119-1)
- Jones HG (1999) Use of thermography for quantitative studies of spatial and temporal variation of stomatal conductance over leaf surfaces. *Plant Cell Environ* 22(9):1043–1055. <https://doi.org/10.1046/j.1365-3040.1999.00468.x>
- Jones HG (2004) Irrigation scheduling: advantages and pitfalls of plant-based methods. *J Exp Bot* 55(407):2427–2436. <https://doi.org/10.1093/jxb/erh213>
- Jones HG, Stoll M, Santos T et al (2002) Use of infrared thermography for monitoring stomatal closure in the field: application to grapevine. *J Exp Bot* 53(378):2249–2260. <https://doi.org/10.1093/jxb/erf083>
- Kang Y, Gao F, Anderson M, et al (2022) Evaluation of satellite leaf area index in California vineyards for improving water use estimation. *Irrig Sci* (in review)
- Knipper KR, Kustas WP, Anderson MC et al (2019) Evapotranspiration estimates derived using thermal-based satellite remote sensing and data fusion for irrigation management in California vineyards. *Irrig Sci* 37(3):431–449. <https://doi.org/10.1007/s00271-018-0591-y>
- Knipper K, Kustas W, Anderson M et al (2020) Using high-spatiotemporal thermal satellite ET retrievals to monitor water use over California vineyards of different climate, vine variety and trellis design. *Agric Water Manag* 241(106):361. <https://doi.org/10.1016/j.agwat.2020.106361>
- Koetz B, Bastiaanssen W, Berger M, et al (2018) High spatio-temporal resolution land surface temperature mission—a Copernicus candidate mission in support of agricultural monitoring. In: *IGARSS 2018—2018 IEEE international geoscience and remote sensing symposium*, pp 8160–8162. <https://doi.org/10.1109/IGARSS.2018.8517433>
- Koetz B, Baschek B, Bastiaanssen W, et al (2021) Copernicus high spatio-temporal resolution Land Surface Temperature Mission: mission requirements document. Technical report. ESA-EOPSM-HSTR-MRD-3276, European Space Agency
- Kondo J, Ishida S (1997) Sensible heat flux from the Earth's surface under natural convective conditions. *J Atmos Sci* 4:54. [https://doi.org/10.1175/1520-0469\(1997\)054<0498:SHFFTE>2.0.CO;2](https://doi.org/10.1175/1520-0469(1997)054<0498:SHFFTE>2.0.CO;2)
- Kustas WP, Norman JM (1999) Evaluation of soil and vegetation heat flux predictions using a simple two-source model with radiometric temperatures for partial canopy cover. *Agric For Meteorol* 94(1):13–29. [https://doi.org/10.1016/S0168-1923\(99\)00005-2](https://doi.org/10.1016/S0168-1923(99)00005-2)
- Kustas WP, Nieto H, Morillas L et al (2016) Revisiting the paper “Using radiometric surface temperature for surface energy flux estimation in Mediterranean drylands from a two-source perspective”. *Remote Sens Environ* 184:645–653. <https://doi.org/10.1016/j.rse.2016.07.024>
- Kustas WP, Anderson MC, Alfieri JG et al (2018) The grape remote sensing atmospheric profile and evapotranspiration experiment. *Bull Am Meteorol Soc* 99(9):1791–1812. <https://doi.org/10.1175/BAMS-D-16-0244.1>
- Kustas WP, Nieto H, García-Tejera O et al (2022) Impact of advection on Two-Source Energy Balance (TSEB) model canopy transpiration parameterization for vineyards in the California Central Valley. *Irrig Sci*. <https://doi.org/10.1007/s00271-022-00778-y>
- Leinonen I, Grat OM, Tagliavia CPP et al (2006) Estimating stomatal conductance with thermal imagery. *Plant Cell Environ* 29(8):1508–1518. <https://doi.org/10.1111/j.1365-3040.2006.01528.x>
- Leuning R (1995) A critical appraisal of a combined stomatal-photosynthesis model for C3 plants. *Plant Cell Environ* 18(4):339–355. <https://doi.org/10.1111/j.1365-3040.1995.tb00370.x>
- Liang S, Wang K, Zhang X et al (2010) Review on estimation of land surface radiation and energy budgets from ground measurement, remote sensing and model simulations. *IEEE J Sel Top Appl Earth Observ Remote Sens* 3(3):225–240. <https://doi.org/10.1109/JSTARS.2010.2048556>
- Liebethal C, Foken T (2007) Evaluation of six parameterization approaches for the ground heat flux. *Theor Appl Climatol* 88(1–2):43–56. <https://doi.org/10.1007/s00704-005-0234-0>
- Lopez G, Behboudian MH, Girona J et al (2012) Drought in deciduous fruit trees: implications for yield and fruit quality. In: *Plant responses to drought stress*. Springer, Berlin, pp 441–459. [https://doi.org/10.1007/978-3-642-32653-0\\_17](https://doi.org/10.1007/978-3-642-32653-0_17)
- Merli M, Magnanini E, Gatti M et al (2016) Water stress improves whole-canopy water use efficiency and berry composition of cv. Sangiovese (*Vitis vinifera* L.) grapevines grafted on the new drought-tolerant rootstock m4. *Agric Water Manag* 169:106–114. <https://doi.org/10.1016/j.agwat.2016.02.025>
- Monteith JL (1995) A reinterpretation of stomatal responses to humidity. *Plant Cell Environ* 18(4):357–364. <https://doi.org/10.1111/j.1365-3040.1995.tb00371.x>

- Nassar A, Torres-Rua A, Kustas W et al (2021) Assessing daily evapotranspiration methodologies from one-time-of-day sUAS and EC information in the GRAPEX project. *Remote Sens.* <https://doi.org/10.3390/rs13152887>
- Nieto H, Kustas WP, Alfieri JG et al (2019a) Impact of different within-canopy wind attenuation formulations on modelling sensible heat flux using TSEB. *Irrig Sci* 37(3):315–331. <https://doi.org/10.1007/s00271-018-0611-y>
- Nieto H, Kustas WP, Torres-Rúa A et al (2019b) Evaluation of TSEB turbulent fluxes using different methods for the retrieval of soil and canopy component temperatures from UAV thermal and multispectral imagery. *Irrig Sci* 37(3):389–406. <https://doi.org/10.1007/s00271-018-0585-9>
- Norman JM, Kustas WP, Humes KS (1995) Source approach for estimating soil and vegetation energy fluxes in observations of directional radiometric surface temperature. *Agric For Meteorol* 77(3–4):263–293. [https://doi.org/10.1016/0168-1923\(95\)02265-Y](https://doi.org/10.1016/0168-1923(95)02265-Y)
- Parry CK, Nieto H, Guillevic P et al (2019) An intercomparison of radiation partitioning models in vineyard canopies. *Irrig Sci* 37(3):239–252. <https://doi.org/10.1007/s00271-019-00621-x>
- Patakas A, Noitsakis B, Chouzouri A (2005) Optimization of irrigation water use in grapevines using the relationship between transpiration and plant water status. *Agric Ecosyst Environ* 106(2):253–259. <https://doi.org/10.1016/j.agee.2004.10.013>
- Priestley CHB, Taylor RJ (1972) On the assessment of surface heat flux and evaporation using large-scale parameters. *Mon Weather Rev* 100(2):81–92. [https://doi.org/10.1175/1520-0493\(1972\)100<0081:OTAOSH>2.3.CO;2](https://doi.org/10.1175/1520-0493(1972)100<0081:OTAOSH>2.3.CO;2)
- Raupach MR (1994) Simplified expressions for vegetation roughness length and zero-plane displacement as functions of canopy height and area index. *Bound Layer Meteorol* 71(1):211–216. <https://doi.org/10.1007/BF00709229>
- Romero P, Fernández-Fernández JI, Martínez-Cutillas A (2010) Physiological thresholds for efficient regulated deficit-irrigation management in winegrapes grown under semiarid conditions. *Am J Enol Vitic* 61(3):300–312
- Santanello JA, Friedl MA (2003) Diurnal covariation in soil heat flux and net radiation. *J Appl Meteorol* 42(6):851–862. [https://doi.org/10.1175/1520-0450\(2003\)042<0851:DCISHF>2.0.CO;2](https://doi.org/10.1175/1520-0450(2003)042<0851:DCISHF>2.0.CO;2)
- Sauer TJ, Norman JM, Tanner CB et al (1995) Measurement of heat and vapor transfer coefficients at the soil surface beneath a maize canopy using source plates. *Agric For Meteorol* 75(1–3):161–189. [https://doi.org/10.1016/0168-1923\(94\)02209-3](https://doi.org/10.1016/0168-1923(94)02209-3)
- Scholander PF, Bradstreet ED, Hemmingsen EA et al (1965) Sap pressure in vascular plants. *Science* 148(3668):339–346. <https://doi.org/10.1126/science.148.3668.339>
- Shaw RH, Pereira A (1982) Aerodynamic roughness of a plant canopy: a numerical experiment. *Agric Meteorol* 26(1):51–65. [https://doi.org/10.1016/0002-1571\(82\)90057-7](https://doi.org/10.1016/0002-1571(82)90057-7)
- Shuttleworth WJ, Wallace JS (1985) Evaporation from sparse crops—an energy combination theory. *Q J R Meteorol Soc* 111(469):839–855. <https://doi.org/10.1002/qj.49711146910>
- Sobrino JA, Jiménez-Muñoz JC, Verhoef W (2005) Canopy directional emissivity: comparison between models. *Remote Sens Environ* 99(3):304–314. <https://doi.org/10.1016/j.rse.2005.09.005>
- Sun L, Gao F, Anderson MC et al (2017) Daily mapping of 30 m LAI and NDVI for grape yield prediction in California vineyards. *Remote Sens.* <https://doi.org/10.3390/rs9040317>
- Taconet O, Olioso A, Mehrez MB et al (1995) Seasonal estimation of evaporation and stomatal conductance over a soybean field using surface IR temperatures. *Agric For Meteorol* 73(3–4):321–337. [https://doi.org/10.1016/0168-1923\(94\)05082-H](https://doi.org/10.1016/0168-1923(94)05082-H)
- Thomas C, Martin J, Goeckede M et al (2008) Estimating daytime subcanopy respiration from conditional sampling methods applied to multi-scalar high frequency turbulence time series. *Agric For Meteorol* 148(8):1210–1229. <https://doi.org/10.1016/j.agrformet.2008.03.002>
- van Leeuwen C, Trégoat O, Choné X et al (2009) Vine water status is a key factor in grape ripening and vintage quality for red Bordeaux wine. How can it be assessed for vineyard management purposes? *OENO One* 43(3):121–134. <https://doi.org/10.20870/oeno-one.2009.43.3.798>
- Wehr R, Saleska SR (2021) Calculating canopy stomatal conductance from eddy covariance measurements, in light of the energy budget closure problem. *Biogeosciences* 18(1):13–24. <https://doi.org/10.5194/bg-18-13-2021>
- Willmott CJ (1982) Some comments on the evaluation of model performance. *Bull Am Meteorol Soc* 63(11):1309–1313. [https://doi.org/10.1175/1520-0477\(1982\)063<1309:SCOTEO>2.0.CO;2](https://doi.org/10.1175/1520-0477(1982)063<1309:SCOTEO>2.0.CO;2)
- Zahn E, Bou-Zeid E, Good SP et al (2022) Direct partitioning of eddy-covariance water and carbon dioxide fluxes into ground and plant components. *Agric For Meteorol* 315(108):790. <https://doi.org/10.1016/j.agrformet.2021.108790>
- Zúñiga M, Ortega-Farías S, Fuentes S et al (2018) Effects of three irrigation strategies on gas exchange relationships, plant water status, yield components and water productivity on grafted Carmenère grapevines. *Front Plant Sci.* <https://doi.org/10.3389/fpls.2018.00992>

**Publisher's Note** Springer Nature remains neutral with regard to jurisdictional claims in published maps and institutional affiliations.

## Authors and Affiliations

Héctor Nieto<sup>1,2</sup>  · María Mar Alsina<sup>3</sup> · William P. Kustas<sup>4</sup> · Omar García-Tejera<sup>5</sup> · Fan Chen<sup>4</sup> · Nicolas Bambach<sup>6</sup> · Feng Gao<sup>4</sup> · Joseph G. Alfieri<sup>4</sup> · Lawrence E. Hipps<sup>7</sup> · John H. Prueger<sup>8</sup> · Lynn G. McKee<sup>4</sup> · Einara Zahn<sup>9</sup> · Elie Bou-Zeid<sup>9</sup> · Andrew J. McElrone<sup>10</sup> · Sebastian J. Castro<sup>10,11</sup> · Nick Dokoozlian<sup>3</sup>

María Mar Alsina  
MariadelMar.Alsina@ejgallo.com

William P. Kustas  
bill.kustas@usda.gov

Omar García-Tejera  
ogarcia@ias.csic.es

Fan Chen  
fan.chen@usda.gov

Nicolas Bambach  
nbambach@ucdavis.edu

Feng Gao  
feng.gao@usda.gov

Joseph G. Alfieri  
joe.alfieri@usda.gov

Lawrence E. Hipps  
Lawrence.Hipps@usu.edu



- John H. Prueger  
john.prueger@usda.gov
- Lynn G. McKee  
Lynn.McKee@ars.usda.gov
- Einara Zahn  
einaraz@princeton.edu
- Elie Bou-Zeid  
ebouzeid@princeton.edu
- Andrew J. McElrone  
andrew.mcelrone@usda.gov
- Sebastian J. Castro  
sjcastro@ucdavis.edu
- Nick Dokoozlian  
Nick.Dokoozlian@ejgallo.com
- <sup>1</sup> COMPLUTIG, 28801 Alcalá de Henares, Spain
- <sup>2</sup> Institute of Agricultural Sciences, CSIC, 28006 Madrid, Spain
- <sup>3</sup> Winegrowing Research, E & J Gallo Winery, Modesto, CA, USA
- <sup>4</sup> Hydrology and Remote Sensing Laboratory, USDA-ARS, Beltsville, MD 20705, USA
- <sup>5</sup> Institute for Sustainable Agriculture, CSIC, 14004 Córdoba, Spain
- <sup>6</sup> Department of Land, Air and Water Resources, University of California, Davis, CA, USA
- <sup>7</sup> Department of Plants Soils and Climate, Utah State University, Logan, UT, USA
- <sup>8</sup> National Laboratory for Agriculture and the Environment, USDA-ARS, Ames, IA, USA
- <sup>9</sup> Department of Civil and Environmental Engineering, Princeton University, Princeton, NJ, USA
- <sup>10</sup> Crops Pathology and Genetics Research Unit, USDA-ARS, Davis, CA, USA
- <sup>11</sup> Department of Viticulture and Enology, University of California, Davis, CA, USA